JOURNAL OF ALGEBRAIC STATISTICS
Volume 13, No. 3, 2022, p. 3894 - 3915
https://publishoa.com
ISSN: 1309-3452

Risk Prediction of Brain Glioblastoma Multiforme Recurrence Using Deep Neural Networks

Mrs. Disha Sushant Wankhede[1*], Dr. Selvarani Rangasamy[2], Dr. Chetan J. Shelke[3],

[1*]Research Scholar, [2,3]Professor, Dept. of Computer Science and Engineering, Alliance college of engineering, University Campus, Anekal, Karnataka 562107

ABSTRACT

Brain Glioblastoma Multiforme (GBM) is one of the most dangerous types of primary malignancy, with a terrible 5-year survival rate of about 4% to 5% and a recurrence rate of up to 90%. Recently, the development of tumour-treating fields has shown positive clinical trial results for further survival extension but no superior efficacy has been observed in the treatment of recurrent GBM. The goal of this research is to discover the Machine Learning (ML) technology used to predict recurrence risk in glioblastoma patients before and after surgery. Radiomics is extensively being applied to advanced and conventional neuro-oncologic imaging data for glial tumours' infiltrating margin detection, postoperative recurrence risk, and overall survival prediction is performed utilizing the rapid evolution of computational methods. Pre-operative Multi-Parametric Magnetic Resonance Imaging (MP-MRI) scans may be used to predict future tumour recurrence and to characterise tumour infiltration. Due to data inhomogeneity, Z-score normalisation and spatial resampling are initially used to address the MR image pre-processing. Subsequently, to address the problem of unbalanced data in medical image semantic segmentation, Recurrent Generative Adversarial Architecture (RNN-GAN) was developed. To construct a stable and validatable preoperative from the tumour area and the peritumoral edema area the research work utilized the CE-T1WI (contrast-enhanced T1-weighted imaging) model to objective response rate (ORR) as well as predict progression-free survival (PFS) in recurrent GBM patients treated with the combination of Bevacizumab and Nivolumab. Additional, to forecast glioblastoma recurrence, the research work proposed a Random forest (RF) model and a Deep neural network is utilized. The system is successfully trained and internally validated, and the patients at high risk of early recurrence are also identified. Subsequently, Inheritable Bi-objective Combinatorial Genetic Algorithm is presented as a feature optimization algorithm to select the relevant factors. The proposed approach has excellent accuracy in predicting GBM patient survival with recurrence rate. The proposed method is evaluated using Python and the proposed method is compared with existing SVM and LR models. The accuracy, specificity, and sensitivity of the proposed method are 3%, 4%, and 5% higher than the existing methods. Subsequently, this research demonstrates that predicted individual patient survival and time to recurrence produces high sensitivity, specificity and accuracy in a retrospective patient cohort.

Keywords*:* Brain Glioblastoma Multiforme, Z-Score Normalisation, Resampling, Recurrent Generative Adversarial Architecture, Nivolumab and Bevacizumab, Progression-Free Survival, and Objective Response Rate.

1. INTRODUCTION

Glioblastoma Multiforme (GBM) is a Grade IV tumour that accounts for approximately 15 to 20% of all initial brain tumours, according to the World Health Organization. In the United States, GBM is the highest prevalence in the 75-84 age group and it increases with age. Rapid mitotic activity, necrosis, microvascular growth, and cellular polymorphism are the most aggressive astrocytic tumour as histological characteristics. The GBM patients have a poor prognosis, based on the advancements in multimodal therapy choices and imaging technology [1]. Patients who do not receive any intervention after diagnosis die soon but patients who receive optimum treatment have an average survival time of 12 to 18 months. Subsequently, long-term survival or only a few cases of curative outcome have been reported [2]. Scott calculated that 2.2% of the cohort existed for more than two years in a comprehensive retrospective investigation. Consequently, with a near-100% final fatality rate, there is less than a 10% for survival rate in 5-years [3]. Subsequently, based on the high likelihood of tumour recurrence, glioblastoma has a poor prognosis [4]. Subsequently, after 32 to 36 weeks of median survival time, it has been indicated that GBM recurrence is unavoidable.

JOURNAL OF ALGEBRAIC STATISTICS
Volume 13, No. 3, 2022, p. 3894 - 3915
https://publishoa.com
ISSN: 1309-3452

Recurrent Glioblastoma Following Nivolumab and Bevacizumab

Under current treatment 4-6, survival rates of patients for two years with recurrent GBM vary from 26% to 33%, and survival rates for five years are less than 10%. Accordingly, to improve GBM patient outcomes, novel approaches are required [5]. Angiogenesis, which is accompanied by elevated expression of vascular endothelial growth factor (VEGF), is the key pathway in GBM pathogenesis. In recurrent GBM patients, some innovative anti-angiogenesis techniques could be a promising treatment [6]. Due to a clear increase in PFS and encouraging radiological response rates in 2009, the Food and Drug Administration (FDA) approved bevacizumab for recurrent GBM patients [7]. In some phases, bevacizumab did not affect overall survival (OS) because of the positive PFS results. In huge RCTs, unlike many other anti-VEGF medications drugs, such as cediranib (VEGF inhibitor), regorafenib (VEGF-TKI), nivolumab (anti-VEGF neutralising antibody), aflibercept (soluble VEGFR), and, bevacizumab produced mixed outcomes in terms of OS and PFS [8]. Consequently, to investigate the results of glioblastoma treatment for recurrent GBM patients, a meta-analysis combining VEGF and anti-VEGF is instantly required [9].

Medical Image Modalities

MRI plays a crucial role in the grading, treatment response assessment of brain tumours, diagnosis, therapy, and other intracranial lesions. In order to evaluate a variety of biophysical parameters of brain tissue quantitatively, several complementary MR imaging techniques have been established [10]. Accordingly, for multi-parametric glioblastoma assessment, only a few have used modern MRI modalities, and numerous studies have been conducted on machine-learning-based glioma classification [11]. Hsieh *et al* used the logistic regression (LR) method to successfully identify glioblastoma from diffuse lower-grade gliomas, with a 91% accuracy and precision of 85% [12]. The availability of experience, facilities, and the clinical challenge at hand should influence the selection of imaging sequences for the multiparametric assessment of brain tumours. In the different analysis and acquisition approaches, they are more accessible and resistant but the information about recurrent tumour issues does not use. Patients' outcomes following recurrent GBM tumour excision have been assessed retrospectively in previous research [14]. Degree of surgical resection, the time interval between the first and second procedures, preoperative KPS score, and age were all found to be substantially linked with OS in at least one of these investigations [15]. In contemplating the surgery of patients, they did not provide any preoperative guidance. Consequently, the article presented a machine learning-based technique for predicting recurrence risk in glioblastoma patients. The remaining part of the work is organized as follows, section 2 portrays the literature survey of the study, and the research problem definition and motivation are exposed in section 3. The proposed research methodology is disclosed in section 4, section 5 elucidates the experimentation and result discussion section, and section 6 reveals the conclusion of the research work.

2. LITERATURE SURVEY

The literature survey is based on the study of glioblastoma recurrence risk prediction among different patients. The utilizes different methods for brain glioblastoma Multiforme recurrence risk prediction.

Clément Acquitter *et al* [16] investigated the potential added value of multiparametric MRI harmonization in improving a radiomics-based categorization challenge. They found that the "scanner effect" is reduced by harmonization, which is caused by enhancing the radiomics-based classification model's predictive performance and differences in multiparametric MRI protocol settings between participating centres. The most accurate classification of tumour development and radionecrosis was achieved using radiomics characteristics retrieved from MRI perfusion. Before any injection of contrast product, had accuracies that were comparable to the perfusion model, the study found that radiomics characteristics recovered from T1-weighted MRI alone.

Kellen Mulford *et al* [17] investigated the usage of radiomics to forecast glioblastoma cell motility. From 31 patients who had their glioblastoma surgically removed, the tissue samples were collected. Specimen cells' time-lapse videos were used to compute mean tumour cell motility. The normalised image volumes extract the 107 radiomics features and the enhancing tumour's border T1-weighted MR images were defined manually. The adaptive lasso technique was used to estimate model parameter coefficients, which were then validated using permutation tests and leave-one-out cross-validation (LOOCV). The prediction model's -values for each parameter estimate were less than 0.0001 and the R-squared value was 0.60.

In clinical routine imaging, to discriminate treatment-related changes (TRC) and recurrent glioblastoma (GBM), the MRI models for single multiparametric are examined by Felix Eisenhut *et al* [18]. Accordingly, they performed the mean, minimum, and maximum cerebral blood volume (CBV) as well as the unselective and selective apparent diffusion coefficient (ADC) in the lesion. CBVlesion to CBVhealthy white matter ratios were calculated at the mean, minimum,

JOURNAL OF ALGEBRAIC STATISTICS
Volume 13, No. 3, 2022, p. 3894 - 3915
https://publishoa.com
ISSN: 1309-3452

and maximum ratios of CBD. Subsequently, for lesion discrimination, all of the data was tested. In an independent patient cohort, multiple logistic regression is used to compile a multiparametric model using data revealing a substantial difference between TRC and GBM and assessed for diagnostic strength. 17 patients are affected with TRC and 17 patients are affected with recurrent GBM, a total of 34 patients were utilized in the study. Consequently, there was no discernible difference in ADC readings between the two entities.

Yae Won Park *et al* [19] distinguish recurrent glioblastoma (GBM) from radiation necrosis (RN) after radiotherapy or concurrent chemoradiotherapy (CCRT) from the diffusion MRI and a high-performing radiomics technique that used ML from conventional is developed. Following radiotherapy or CCRT, in the training set, 86 GBM patients were enrolled and within the radiation field on follow-up MRI, a contrast and new enhancement is presented. Either clinicoradiologically or pathologically (23 RN and 63 recurrent GBM), a diagnosis was made. The test group included 41 patients (18 with RN and 23 with recurrent GBM) from a separate hospital. A 263 radiomic features were extracted from conventional MRI sequences (postcontrast T1-weighted and T2-weighted images) and ADC. Oversampling approaches were utilized to train several ML models with combinations of MRI sequences, which were then confirmed in the test set, which is performed after feature selection.

Using machine-learning techniques, Samy Ammari *et al* [20] found a biomarker collected from clinical and MRI data that might predict PFS and OS in GBM patients treated with bevacizumab. Radiomics data from gadoliniuminjected MRI images and pre-treatment T2 FLAIR, as well as clinical characteristics, were analysed in a group of 194 recurrent GBM patients (ages 18–80). Subsequently, at 9, 12, and 15 months, binary classification models for OS were tested. The OS was successfully stratified using their classification models. Subsequently, for the 9-, 12-, and 15- month endpoints, the AUCs on the test sets, are 0.78, 0.85, and 0.76 and on the training sets, the AUC is 0.79, 0.82, and 0.87.

Bin Sheng Wong *et al* [21] proposed that a microfluidic technique for quantifying proliferation and cell migration might be used to categorize glioblastoma patients based on their PFS. The ability of primary glioblastoma cells is assessed to proliferate (as measured by the protein biomarker Ki-67) as well as squeeze into microfluidic channels, simulating brain parts parenchyma's narrow perivascular conduits and white-matter parenchyma. With an 86% accuracy, the test retrospectively classified 28 patients based on PFS (short-term or long-term), based on survival, and prospectively classified five more patients, and predicted time to recurrence. The highly motile cells' RNA sequencing identified differentially expressed genes that were linked to a bad prognosis. To predict patient-specific outcomes, the amounts of proliferation and cell migration can be used which implies in the findings.

The formation of glioblastoma multiforme (GBM) with similar imaging characteristics to human GBM is examined by Seunghyun Lee *et al* [22] in an orthotopic xenograft canine GBM model using multiparametric MRI. In a total of 15 surgical success instances, with dynamic susceptibility CE perfusion-weighted imaging (PWI), diffusion-weighted imaging (DWI), and conventional MRI, at one week and two weeks after surgery, the multiparametric MRI was performed. On the histologic specimen, the tumour's microvessel density (MVD), the presence of tumour cells and the necrotic area fraction were all evaluated. Subsequently, between the histologic parameters and imaging, a Spearman correlation analysis was performed.

In order to predict recurrence patterns in glioblastoma, two different neural network models are proposed by Ka Young Shim *et al* [23] using high-dimensional radiomics profiles based on perfusion MRI for each patient in the validation set: 0.864 (0.726–0.976) for distant recurrence, for local recurrence, is 0.969 (0.903–1.000), (95% confidence interval) for the area under the curve (AUC). In contrast to research that looks at only group differences, this opens up the possibility of providing tailored medicine. In order to intratumoral perfusion heterogeneity, for each recurrence pattern, the salient radiomic features are related and discovered by interpretable deep learning.

A post-surgery multiparametric magnetic resonance-based support vector machine (SVM) technique is developed by Yi Lao *et al* [24], which included an estimate of stem cell niche (SCN) proximity. The analysis of 50 patients with recurrent GBM begins approximately two months prior to clinically diagnosed recurrence , this data is utilized for post-surgery MRI scans. In order to recognize regions with a High Risk of Recurrence (HRRs), a proximity-based estimator was used and to offer voxel-wise prediction in HRRs, an SVM classifier was used. During training and testing, the cohort was randomly divided into two groups of 40% and 60%. Subsequently, for earlier recurrence prediction, the learned SVMPE was projected to an earlier time point.

The efficacy in patients with recurrent glioblastoma was studied by Beatrice Detti *et al* [25], with the impact on acceptable toxicity profile and survival endpoints. Subsequently, recurring disease must be treated systemically at least once , high-grade glioma was treated at their institution that underwent histological or radiological progression for the

JOURNAL OF ALGEBRAIC STATISTICS
Volume 13, No. 3, 2022, p. 3894 - 3915
https://publishoa.com
ISSN: 1309-3452

patients' retrospective review data. Until the unacceptable toxicity or the disease progression, combining chemotherapy with bevacizumab was common. OS and PFS were measured utilizing the bevacizumab regimen. In PFS, performance status, usage of corticosteroids and age at diagnosis (< 65 or > 65 years) was strongly associated during bevacizumab therapy.

This study provides an overview of recent advances in MRI sample processing for early detection of brain tumours and gliomas utilising a deep learning technique by Disha Wankhede *et al* [27]. In MRI image processing, the benefit of learning capability and finer processing efficiency has acquired an edge, allowing for improved processing efficiency and accuracy in early diagnosis. The usefulness of picture coding based on chosen characteristics and state-of-the-art processing in diagnosis has been demonstrated using a deep learning technique. The accuracy of the MRI sample processing assessment goal was higher than that of comparable current techniques. The current technique for MRI diagnosis is discussed in terms of recent trends, benefits, and limitations.

This study discusses recent advances in medical diagnostics and deep learning applications for heart disease detection by Trupti Bhandare *et al* [28]. The application, database, and learning system employed in the automation process are examined, and the evolution of the deep learning technique for medical data analysis is explained.

In this paper, weighted clustering is proposed as a diagnostic method for heart disease by Trupti Bhandare *et al* [29].

A new model for glioblastoma survival prediction based on CNN features was created in the paper by Disha Wankhede *et al* [30].

3. RESEARCH PROBLEM DEFINITION AND MOTIVATION

Glioblastoma has a terrible prognosis, with a less than 10% of survival rate for 5-years. Following standard-of-care surgical radiotherapy, temozolomide, and resection, nearly all patients have a recurrence. Extremely, the biology of recurrent glioblastoma is relatively unknown but the majority of current glioblastoma research focuses on primary tumours, which are those that are freshly identified and untreated tumours. Subsequently, this knowledge gap can be credited to several factors. A large-scale systematic tissue banking is hampered for the surgical treatment for this only 20–30% of recurrent glioblastomas are accessible. In comparison to original glioblastoma tissues, recurrent glioblastoma tissues have less viable tumour cell concentration and more necrotic tissue. Subsequently, for recurrent glioblastoma, currently, there is no conventional treatment and during the initial diagnosis, most patients die within 12–15 months. In this patient population, this emphasises the importance of innovative therapeutic strategies.

In the treatment of glioblastoma, immunotherapy has been used to increase antitumor immune response in the area of recent research. T-cell costimulatory cytokines on activation and major histocompatibility complex III antigens are expressed by resident macrophages and the central nervous system (CNS) in this accumulating evidence suggests that immune cells can function, proliferate, and enter. In patients with recurrent GBM, antibodies targeting immunological checkpoints have demonstrated little efficacy. These data, as well as results from murine glioma models that demonstrate checkpoint inhibitors improve survival, imply that immune checkpoint blockade could be a viable therapy option for glioblastoma. In order to boost the immune response to tumour cells, preclinical research has shown that moderate hypofractionated radiation works in tandem with immunotherapy. Accordingly, this inspires researchers to use ML and quality improvement to examine the efficacy of bevacizumab and nivolumab in patients with GBM recurrence.

4. PROPOSED RESEARCH METHODOLOGY

Glioblastoma is a WHO grade IV brain tumour that causes patients to have a poor OS. Response rate and PFS prediction of recurrent glioblastoma (GBM) patients are greatly wanted by oncologists and clinicians for therapeutic planning and precise surgery. A range of imaging variables collected from many MR scans is used for radiomic research aims to predict disease prognosis, therefore useful information is offered for individualised treatment. PFS and ORR are used to measure the delay of tumour recurrence and tumour shrinkage is a potentially important supplementary goal if they correspond with improvements in either patient well-being or OS. Subsequently, for glioblastoma (GBM), historically limited consistency is established and for other malignancies, these links have been established regularly.

JOURNAL OF ALGEBRAIC STATISTICS
Volume 13, No. 3, 2022, p. 3894 - 3915
https://publishoa.com
ISSN: 1309-3452

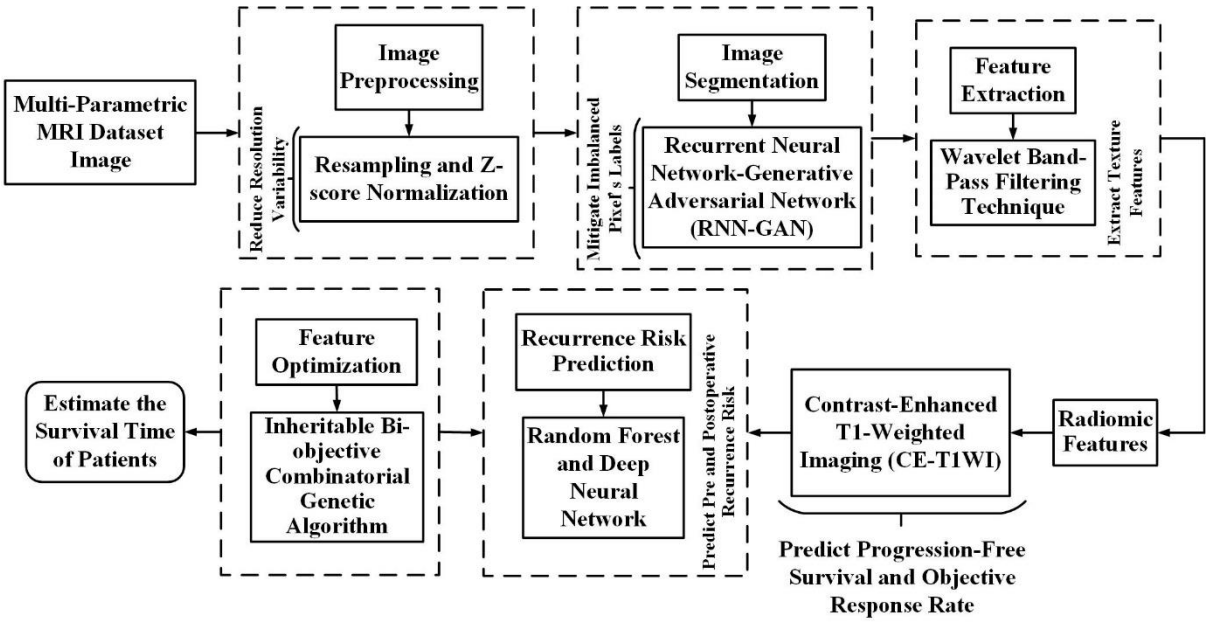

Figure 1: Block Diagram of the Proposed Work

Figure 1 depicts the general framework of the proposed strategy. Pre-processing, Z-score normalisation and spatial resampling; step 2: recurrent generalised adversarial network tumour segmentation; step 3: texture feature extraction (FE) using wavelet band-pass filtering; step 4: random forest to forecast recurrent glioblastoma are the four steps involved in this research. Among the glioblastoma patients treated with a combination of Bevacizumab and Nivolumab, this study aimed to assess the efficiency of the pre and post operative recurrence risk. In the training cohort, there were 84 patients and in the testing cohort, there were 42 patients, separated based on pretherapy imaging date. From contrast-enhanced T1-weighted images, tumour volumes of interest were segmented. In patients with gliomas, to determine their relationships with response OS and PFS, the radiomic feature-based MRI signatures were extracted from multiparametric MRI data. The random forest method is used for recurrence rate prediction for GBM patients based on multi-scale textural traits. CE-T1W-MRI imaging data was used to extract the features from MRIs. The following subsections detailly explain each stage.

a. Patient Population

It was approved by the local Institutional Review Board and no written informed consent was required for this retrospective study. Consequently, for this investigation, a total of 45 patients were gathered. Except for Grade I gliomas, for patients with pathologically confirmed newly diagnosed gliomas; before any treatment or surgery, multiparametric MRI examinations were performed. Based on a 10-fold cross-validation, the area under the receiver operating characteristic (ROC) curve of this model was obtained and an ML method (multivariate random forest and univariate logistic regression) is used to develop a prediction model. The machine learning method's performance was compared to Bevacizumab and Nivolumab. Finally, 173 patients and their clinical features were enrolled.

i. Multi-Parametric MRI Dataset

The features obtained from a multiparametric MRI-based radiomic analysis can be utilised to inform imaging prediction, diagnosis, and prognostic evaluation in precision medicine treatment selection. DWI, PWI, and cMRI are included in the MP-MRI acquisition protocol for all patients. Before and after contrast injection, cMRI consisted of a 3-dimensional T1-weighted gradient-echo sequence (MPRAGE) with isotropic voxels and with isotropic voxels, a 3-dimensional T2-weighted inversion recovery sequence (FLAIR).

b. Image Pre-Processing

Pre-processing is frequently required after image acquisition to reduce artefacts and bias in neuroimaging data caused by inhomogeneous magnetic fields in MRI, as well as body motions including respiration motions and head movements. Subsequently, it includes picture pixel size resampling to reduce resolution fluctuation, bias field correction,

JOURNAL OF ALGEBRAIC STATISTICS
Volume 13, No. 3, 2022, p. 3894 - 3915
https://publishoa.com
ISSN: 1309-3452

intensity normalisation, image co-registration, and skull stripping (i.e. brain segmentation to exclude surrounding structures such as contents, orbital, bone, and so on).

i. Resampling Image Pixel

In radiomics research, interpolation and pixel size resampling are required pre-processing steps, the impact of pixel size and slice thickness on radiomic characteristics is not well understood. Subsequently, for interpolation and pixel size resampling, ICC was utilised to test feature robustness. The following equation is the ICC:

$$ICC = \frac{MS_R - MS_E}{MS_R + (k-1)MS_E + \frac{k}{n}(MS_C - MS_E)} \tag{1}$$

Where the number of patients is denoted as n, MS_R denotes the mean square for feature values, the mean square for repeated measures is described as MS_C, the number of repeated acquisitions is k, the mean square for error is represented as MS_E. The reliability and repeatability of numeric measurements in groups are assessed using the ICC method. In addition to comparisons between more than two groups of variables, it has the benefit of being able.

ii. Z-Score Normalization

The Z-Score approach involves dividing each voxel value by the corresponding standard deviation after subtracting the mean intensity of the region or an entire image of interest. The brain mask B for image I is used in Z-score normalisation to obtain the standard deviation σ_{zs} and mean μ_{zs} of the intensities inside the brain mask. The image is then normalised by Z-score.

$$I_{z-score}(x) = \frac{I(x) - \mu_{zs}}{\sigma_{zs}} \tag{2}$$

In order to guarantee that voxels across images have relationships and similar spatial placement, spatial pre-processing is necessary before training and it is significant as CNNs do not typically take into consideration metadata associated with medical images. Resampling is a common spatial pre-processing procedure used in medical imaging (e.g., for all training samples make voxel spacing isotropic).

c. Recurrent Generative Adversarial Network for Image Segmentation

The recurrent generative adversarial network is presented in this paper for medical image semantic segmentation. The algorithm combined adversarial loss with categorical accuracy loss to mitigate uneven pixel labelling. The generative model g in a traditional generative adversarial network decides to learn a mapping from a random noise vector z to an output image y, $g: z \to y$. Rather than the generator x_{fake}, a discriminative model D calculates the likelihood of a sample coming from the training data x_{real}. Two-player mini-max game with a value function $V(g,d)$ is the GAN objective function.

$$\min_g \max_d \; V(d,g) = E_y[\log d(y)] + E_z[\log(1 - d(g(z)))] \tag{3}$$

The conversion of a set of 2D medical images x_i to the semantic segmentation of matching labels $y_{i_{seg}}$; $g: x_i, z \to \{y_{i_{seg}}\}$ is learned by the generative model, in this proposed RNN-GAN network. In order to regulate whether the predicted label is real or fake, the discriminator uses the ground truth and the generator's output while the generator predicted segmentation at the pixel level.

JOURNAL OF ALGEBRAIC STATISTICS
Volume 13, No. 3, 2022, p. 3894 - 3915
https://publishoa.com
ISSN: 1309-3452

$$L_{adv} \leftarrow \min_{g} \max_{d} V(d,g) = E_{x,y_{seg}}\left[\log d\left(x, y_{seg}\right)\right] + E_{x,z}\left[\log\left(1 - d\left(x, g\left(x,z\right)\right)\right)\right] \quad (4)$$

Furthermore, By allocating a greater cost to the less represented group of pixels, the article used mixed categorical accuracy loss l_{acc} (4) to minimise imbalanced training data, during the learning process increasing their importance. The final adversarial loss for the RNN-GAN semantic segmentation challenge is then determined (5).

$$L_{RNN-GAN}(d,g) = L_{adv}(d,g) + L_{L1}(g) + L_{l_{acc}}(g) \quad (5)$$

The proposed RNN-GAN is trained with complimentary masks in addition to ordinary masks to limit the influence of imbalanced pixels' labels on medical images. Categorical cross-entropy loss with the adversarial loss gives an unbiased estimator for minimising the risk because the system assumes transition probabilities are identical. In addition to typical losses, complimentary labels can yield more accurate results for a semantic segmentation task.

Due to their irregular morphologies and infiltrative growth patterns, which can be seen as gradual changes in morphology and intensity on MRI, however, brain tumour segmentation is particularly difficult, especially in diffuse gliomas. Consequently, appearance with similar grey levels, precise segmentation might be challenging when the imaging sequence is not dedicated to tumour identification, and two separate lesions may appear almost identical.

d. Radiomic Feature Extraction

More elements from derived and original images are added to the radiomics signature to develop it. In terms of survival, more features based on the Wavelet transform have greater significance coefficients, which influenced the radiomics signature model. Based on FE may accurately and quickly estimate survival time (PFS and OS) with speed and precision beyond the scope of human visual analysis (10, 19, 20), that previous research has demonstrated multiscale texture analyses of MRI.

i. Contrast-Enhanced T1-Weighted MRI Imaging

The workhorse of brain tumour imaging is contrast-enhanced T1-weighted MRI imaging. The margins of dural-based lesions and most brain metastases are precisely depicted and it is simple to perform. The tumours frequently have infiltrative components or are non-enhancing, it is less reliable in the case of primary brain neoplasms, notably gliomas. Due to that, it clearly distinguishes aberrant signals from normal brain parenchyma, T2 fluid-attenuated inversion recovery (FLAIR) imaging is frequently used in these situations. T2 FLAIR imaging is particularly useful for determining tumour extent because low-grade gliomas rarely demonstrate vasogenic oedema. On T2 FLAIR sequences, both are hyperintense, the T2 FLAIR imaging has difficulties in high-grade gliomas since it cannot effectively distinguish infiltrating tumours from vasogenic oedema. In order to distinguish recurrent/residual tumours from post-treatment alterations, improved imaging techniques are frequently used. MR spectroscopy, PWI, and DWI are the most frequent advanced imaging techniques. A tumour is correctly separated from post-treatment changes, all of them can usually allow the radiologist to use for a thoughtful synthesis, subsequently, none of these techniques has proven very specifically. In order to determine the radiomic characteristics, as the input volume, the preoperative T1W contrast-enhanced lesion was manually sketched. Nine separate MR sequences yielded 87 radiomic features, including filtered wavelet, and first, and second-order analysis. In the study, a total of 11 shape features were employed.

ii. Wavelet Band-Pass Filtering Technique

In a family of scaled and translated functions $\psi_{m,n}(r)$, the wavelet transforms correlates to the disintegration of a quadratic integrable function $S(x)\varepsilon L^2(Q)$.

$\psi_{m,n}(r) = m^{-1/2}\,\psi\left(\frac{r-n}{m}\right)$. The function $\psi(x)$ is referred to as the wavelet function, and it exhibits bandpass behaviour. The wavelet coefficients $d_{m,n}$ are calculated in the following way:

JOURNAL OF ALGEBRAIC STATISTICS
Volume 13, No. 3, 2022, p. 3894 - 3915
https://publishoa.com
ISSN: 1309-3452

$$d_{m,n} = \frac{1}{\sqrt{2}} \int S(x) \psi * \frac{x-n}{m} dx \tag{6}$$

Where the entire conjugate function is represented as $k\ \varepsilon\ Q^{+}$, $k\ \varepsilon\ Q^{+}$, and $*$. In terms of shifted and dialled versions of a prototype bandpass wavelet function and low pass scaling function's $R(z)$ shifted versions, a single-dimensional signal $y(z)$ is described by the discrete wavelet transform (DWT):

$\psi(r)$ can be represented as:

$$\psi(r) = \begin{cases} 1 & 0 \le r < \frac{1}{2} \\ -1 & \frac{1}{2} \le r < 1 \\ 0 & otherwise \end{cases} \tag{7}$$

The Haar function $\psi_{m,n}$ is defined on the real line Q by the formula $\psi_{m,n}(-r) = 2^{\frac{m}{2}} \psi\left(2^{m} r - n\right),\ r\,\varepsilon\, Q$ for each pair m, n of integers in Z .

The three subbands provide information and one provides an approximation, that the single-dimension DWT divides the image into sub-images. The image obtained through approximation will resemble the original in appearance but will vary in size. According to low resolution, horizontal a diagonal component, vertical, the DWT divides an image. The image is divided into several subbands by the high and low pass filters. The final consequence generated from the local mean is used for the image approximation method when considering the DWT. The procedure is stopped and the mean of the final result is determined when the approximation image is obtained.

Subsequently, the measured vibration signal's convolution with the wavelet is given by

$$s_b(t) = s(t) \times h_c(t) \tag{8}$$

Where $s_b(t)$ is the component of the original signal $s(t)$ in the passband $f_L \sim f_H$.

The wavelet as a band-pass filter provides a lot of advantages. Its design and adjustment are simple and convenient. Appropriate filter characteristics can be obtained by adjusting a and Δf depending on the actual requirements, selecting suitable f_L and f_H , defining the frequency band to be analysed. The wavelet-based band-pass filter was carefully developed to have zero phase shift. While also performing envelope demodulation in one step, the wavelet cluster as a digital filter generates the analytical signal.

A protocol for extracting features has been followed to ensure that retrieval accuracy is reflected for each technique. All of the rudimentary elements are combined as this architecture demonstrates.

e. Recurrence Risk Prediction

Predicting the probability of recurrence of glioblastoma cancer is important since it improves survival rates and lowers patient mortality. To forecast the probability of brain cancer recurrence over a five-year or longer length of time depending on the outcome attribute is the aim of this research. The performance of the RF and DNN techniques is estimated to address this issue. Accordingly, for estimating the relevance of features and balancing data, RF is a powerful tool that is utilized in classification tasks.

i. Random Forest for Classification

In the training cohort, an RF classifier was utilised to differentiate patients who survived less than or more than the 50th percentile of PFS. Several decision trees are integrated into a single predictive algorithm for the RF algorithm, it

JOURNAL OF ALGEBRAIC STATISTICS
Volume 13, No. 3, 2022, p. 3894 - 3915
https://publishoa.com
ISSN: 1309-3452

is a type of ensemble learning system. By bagging, each decision tree was trained using data. The ability to estimate generalisation error from the calculation of an out-of-bag error and the ability to use high-dimensional data (where the number of characteristics is much greater than the number of patients) are the advantages of RF. The mean prediction error in each patient within the training set, considering just the trees that did not have that patient in the bagged sample, was designated as the out-of-bag error. The generalisation error converges to a limit as the forest expands by adding more decision trees. The RF approach is resistant to overfitting because of the large number of decision trees in the forest, making it excellent for heterogeneous datasets like those containing patients with recurrent glioblastoma. The ROC curve analysis is used to compute the AUC based on these all features were first evaluated for their predictive value. In the random forest algorithm, the top 128 features were fed. The trained RF algorithm was used to validate the RF algorithm on the testing cohort.

ii. Deep Neural Network (DNN) Technique

A DNN is employed in this study to forecast the probability of glioblastoma recurrence. The hidden layers are used to create a hierarchy in DNN designs. The combination of lower-level information from each layer extracts higher level features implicitly. An input layer, many hidden layers, and an output layer make up a DNN model. The layers' units are all fully connected. One or more dimensions of data make up the input layer with an input vector x. The outputs' weighted sum for the previous layer h^{k-1} is utilized to determine the output h_j^k for the layer k comprising j units (especially $h^0 = x$).

$$g^k = W^k h^{k-1} + b^k, 1 \le k \le N \tag{9}$$

$$h^k = f\left(g^k\right) \tag{10}$$

The k^{th} weight matrix between k^{th} layer and $(k-1)^{th}$ layer can be represented as W^k, k^{th} the layer b^{th} is the bias vector. Hidden units are activated via hyperbolic tangent (TANH) activation $f(.)$ and N are the number of layers (here $N=5$, including the output layer), which naturally capture the nonlinear relations within the data. Simultaneously, in the DNN structure, the softmax function for the output layer (N^{th} layer) is employed as an activation function and is specified as:

$$a^N = \frac{\exp\left(h^N\right)}{\sum_j \exp\left(h_j^N\right)} \tag{11}$$

Subsequently, using a truncated normal distribution, the weights across layers are initialized, which is described by

$$W \sim T\left[-\sqrt{\frac{2}{n_i + n_0}}, \sqrt{\frac{2}{n_i + n_0}}\right] \tag{12}$$

Where the number of units' input and output can be represented as n_i and n_o, respectively. The architecture diagram of the DNN is portrayed in figure 2. Subsequently, it consists of input layers, hidden layers, and output layers.

JOURNAL OF ALGEBRAIC STATISTICS
Volume 13, No. 3, 2022, p. 3894 - 3915
https://publishoa.com
ISSN: 1309-3452

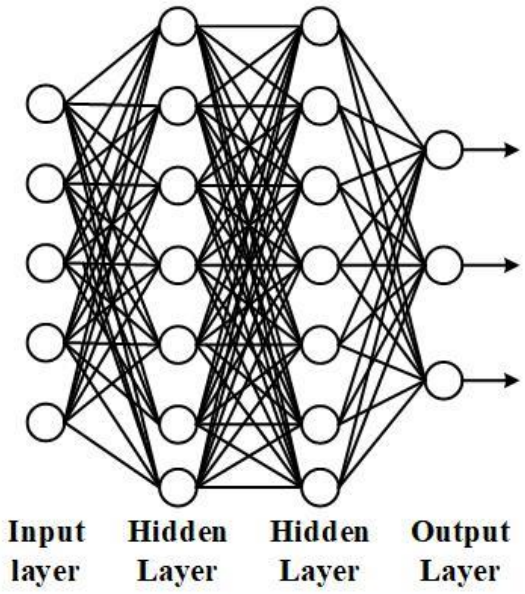

Figure 2: Basic Architecture Diagram of Deep Neural Network

In this work, the glioblastoma recurrence risk prediction task is a binary classification task (short-term survival and long-term survival), and in the final output layer, it uses cross-entropy loss as the DNN model's objective function. L2 regularisation is also included in this loss function, which is extensively utilised in deep learning studies, to further minimise the overfitting of the deep learning model. Finally, the proposed DNN approach, which is defined as follows, tries to minimise the loss function.

$$L(y_t\ \hat{y}_t)=-\frac{1}{N}\sum_{i=0}^{N}[y_t(i)\log\hat{y}_t(i)-(1-y_t(i))\log(1-\hat{y}_t(i))]+\frac{1}{2}\lambda\sum_{k=1}^{K}\sum_{j=1}^{n_k}\sum_{i=1}^{m_k}{w_{ij}^k}^2 \qquad (13)$$

Where L measures errors between predictive scores and the actual labels. $y_t(i)$ is the actual label for the i^{th} class, $\hat{y}_t(i)$ is the predictive scores obtained from the output layer of the method. N is the batch size. $W^k=\{w_{ij}^k\}_{m_k\times n_k}$ is the k^{th} weight matrix and K is the number of weight matrices in the DNN model (here $K=5$).

A common issue in training a DNN model is named “internal-covariate-shift”, which is that input distributions change in each layer during training due to the update of parameters from previous layers. Finally, a DNN model employed in our work comprises one input layer, four hidden layers and an output layer. Batch normalization is added to each hidden layer and a dropout is added before the output layer. Consequently, this model classifies and predicts the glioblastoma recurrence risk prediction of cancer patients.

iii. Inheritable Bi-objective Combinatorial Genetic Algorithm (IBCGA)

IBCGA is an evolutionary approach for solving large-parameter combinatorial optimization problems. Additionally, for obtaining a comprehensive set of non-dominating solutions, IBCGA employs an Orthogonal Experimental Design (OED) based on an orthogonal array. Simultaneously, the impact of numerous factors on the response variable is examined by OED. The OED is used to find the best level combination and the level of an element determines its value. Subsequently, due to the analysis, minimising the number of levels needed and in a balanced manner, an orthogonal array can compare levels of items. While the column illustrates which elements can be changed for each combination, each row in an orthogonal array displays the level of components in a given combination. The main effect of one element has no bearing on the main effect of another element and the main effect is denoted as the primary effect of one element on the response variable. For example, an orthogonal design with p rows and $p-1$

JOURNAL OF ALGEBRAIC STATISTICS
Volume 13, No. 3, 2022, p. 3894 - 3915
https://publishoa.com
ISSN: 1309-3452

columns having two levels (values of elements) is designated as $L_P\left(2^{P-1}\right)$. The main effect of an element x having a level y is denoted as

$$S_{xy} = \sum f_k . F_k , \quad k\ 1,\ldots,P \tag{14}$$

$$x = 1,\ldots,P-1 \tag{15}$$

$$y = 1,0 \tag{16}$$

In equation (14), f_k is the value of function which is usually the prediction accuracy obtained from the combination k and $F_k = 1$, if, in combination k, the level of element x is y else $F_k = 0$. Here, $S_{x1} > S_{x0}$, if level 1 of an element x is preferable to level 0 of an element x in maximizing the objective function. The variable with the highest main effect difference $\left(MED = \left|S_{x1} - S_{x0}\right|\right)$ is the most impacting one. IBCGA chooses important MiRNAs from a search space of $C(n,r)$ based on MED, where the range of r is initially provided. Tenfold cross validation is used as the fitness function and a set of solutions, X_P, is obtained where $p = p_{start}, p_{start+1}, \ldots, p_{end} . p_{start}$ and p_{end} is initially specified. The IBCGA algorithm's major steps are shown in the pseudo-code represented as following table 1.

Table 1: Inheritable Bi-objective Combinatorial Genetic Algorithm

Input: Expression profiles
Output: Reduced set consisting of key
Begin
$t <- 0$
Generate the initial population randomly with n binary genes having $p1'$ and $n-p0'$ where $p = p_{start}$.
Set the fitness function as the accuracy of prediction concerning 10- fold cross-validation.
While (! Stop condition) do
Select best fit individuals using tournament selection to form the mating pool.
Perform orthogonal cross over on pair of parents selected.
Apply mutation on randomly selected individuals.
Evaluate the individuals.
Replace the least performance population with new individuals.
If $p < p_{end}$, transform one gene bit chosen randomly from 1 to 0.
$t <- t+1$
End While.

Subsequently, different combinations were applied on trial and error bases and the algorithm performed with the highest accuracy with the above parameter setting. IBCGA output was further developed by applying factor analysis for picking out the most relevant MiRNAs.

5. EXPERIMENTATION AND RESULT DISCUSSION

The results of the proposed model for intelligent detection of brain tumours and their types using a Random forest and Deep neural network. RF-DNN based smart healthcare system is planned for accurate recognition and classification of brain tumours. The dataset was collected from Kaggle, which comprised four classes, including one no-tumour and three tumour types. The sample images for brain tumour is depicted in figure 3, respectively.

JOURNAL OF ALGEBRAIC STATISTICS
Volume 13, No. 3, 2022, p. 3894 - 3915
https://publishoa.com
ISSN: 1309-3452

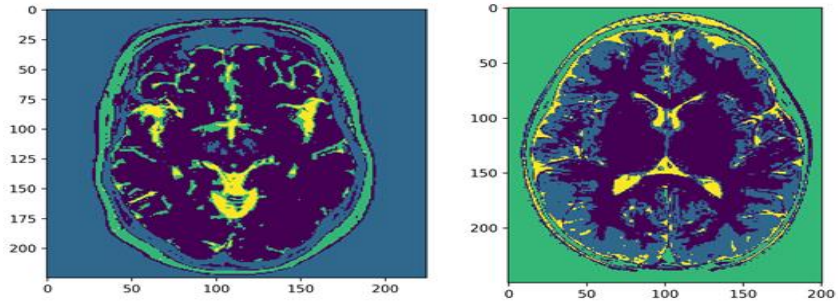

Figure 3: Sample Images for MRI Brain Tumour

The proposed model used 253 MRI brain tumour images for the pituitary, meningioma, and glioma classes, respectively. The training and validation phases of the proposed model are separated. 81% of input images are chosen from each class in the training phase, and in the validation phase, 19% are used. The model's efficiency is evaluated by miss rate (MR) and accuracy (ACC).

Table 2: Simulation System Configuration

Simulation System Configuration	
Operation System	Windows 10 Home
Memory Capacity	6GB DDR3
Processor	Intel Core i5 @ 3.5GHz
Simulation Time	10.190 seconds

The simulation system configuration of the proposed work is portrayed in table 2. Subsequently, the proposed technique is evaluated and tested. The proposed work operates under windows 10 home and its memory capacity is 6GB DDR3. Additionally, it utilizes an Intel Core i5 @ 3.5GHz processor and the simulation time of the work is 10.190 seconds.

Statistical Analysis

The Kaplan- Meier method was employed to evaluate PFS and OS predictions. Subsequently, for survival analysis, the proposed method was calculated using a significance level of P 05 for a 2-sided comparison.

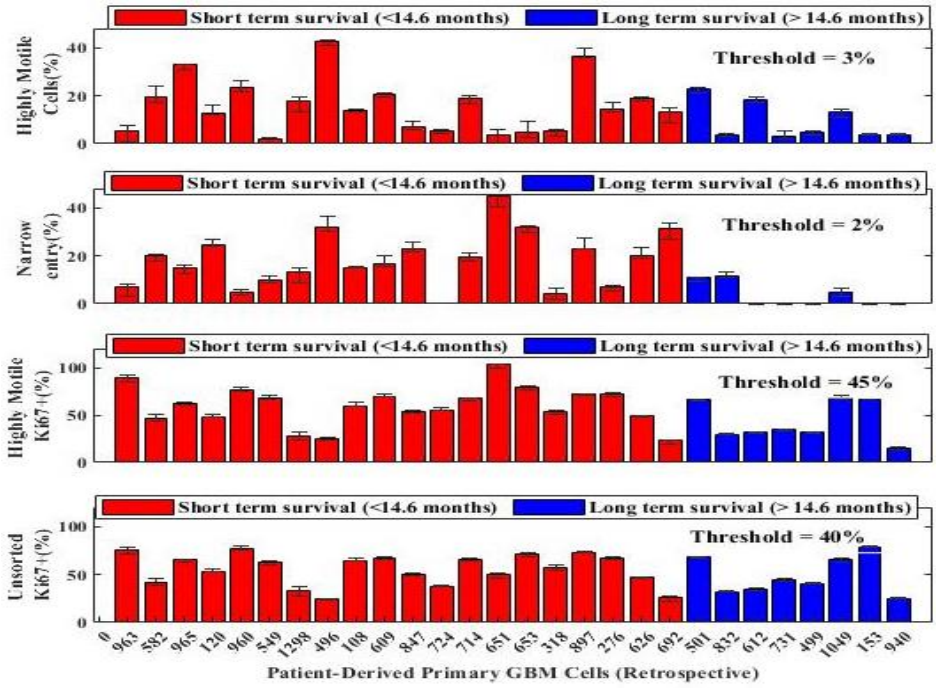

Figure 4: Survival Analysis Using Proposed Method

JOURNAL OF ALGEBRAIC STATISTICS
Volume 13, No. 3, 2022, p. 3894 - 3915
https://publishoa.com
ISSN: 1309-3452

Figure 4 illustrates the Survival analysis of GBM patients. Subsequently, it described Patient-Derived primary GBM Cells, and it is predicted for long term and short term survival. Subsequently, the analysis is utilized for narrow entry, highly motile cells, highly motile Ki67, and Unsorted Ki67. The survival analysis is represented as < 14.6 months as short term survival and > 14.6 months represented as long term survival. Accordingly, the threshold value for the proposed work is 3%, 2%, 45%, and 40% for narrow entry, highly motile cells, highly motile Ki67, and Unsorted Ki67. Subsequently, the different patients with long time survival are less than the short time survival, respectively.

Each imaging feature was subjected to ROC analysis in the classification of both long and short-term survival. Shape, shape, texture, and texture were the highest performing individual features for pre-therapy features predicting PFS, pre-therapy features predicting OS, pre-and post-therapy features predicting OS, and pre-and post-therapy features predicting OS excluding early progresses.

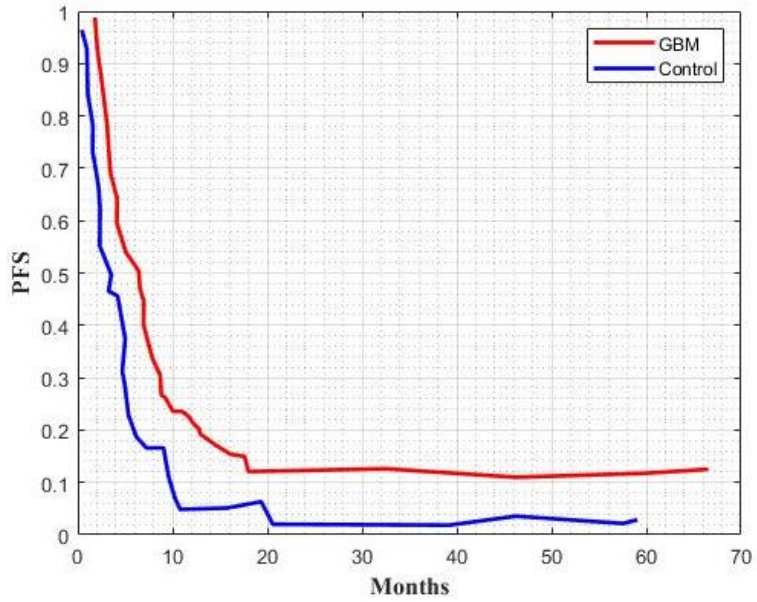

Figure 5: Progression-Free Survival

The PFS of the proposed model is depicted in figure 5. PFS; is defined as the time from randomization to disease progression or death from any cause). Subsequently, for different months, PFS was not substantially different between the GBM and the control.

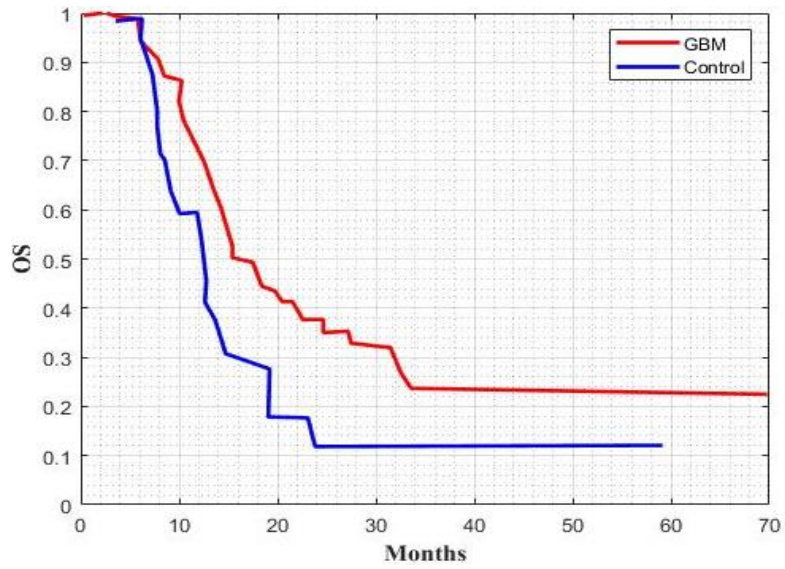

Figure 6: Overall Survival of the Proposed Work

JOURNAL OF ALGEBRAIC STATISTICS
Volume 13, No. 3, 2022, p. 3894 - 3915
https://publishoa.com
ISSN: 1309-3452

Figure 6 represents the predict the OS using the proposed method. The Kaplan-Meier method was used to calculate the OS, it was a primary outcome and it is defined as the time from randomization to death from any cause. Between the GBM and the control, the OS did not differ significantly.

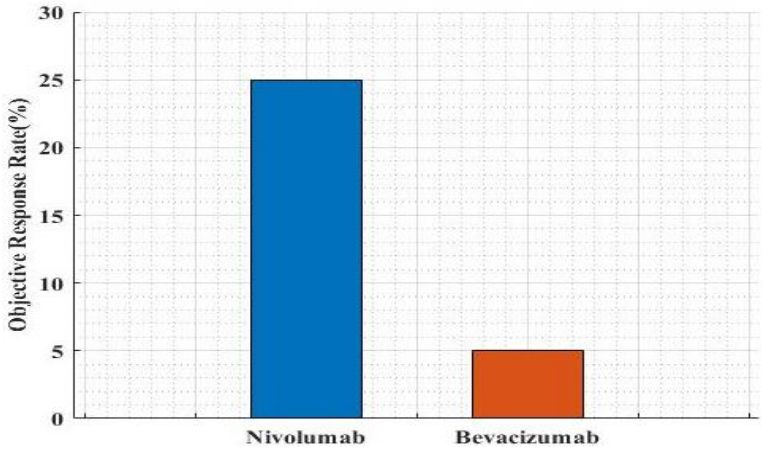

Figure 7: Object Response Rate

The objective response rate of the proposed work is portrayed in figure 7. Accordingly, it represents patients on nivolumab treatment had a significantly better objective response rate than those on bevacizumab treatment. Consequently, this means that more patients responded to treatment with nivolumab than to treatment with bevacizumab.

Validation

Based on the experienced radiologist, the pathological tissue regions' segmentation results were compared to manual segmentation. In terms of spatial alignment between manual and semi-automated segmentation, the Dice score was utilized to compare:

$$Dice_{\{tissue\}} = 2 \times \frac{A_{\{tissue,NB\}} \bigcap A_{\{tissue,man\}}}{A_{\{tissue,NB\}} + A_{\{tissue,man\}}} \tag{17}$$

Where $A_{\{tissue,man\}}$ is the area manually segmented by the radiologist for the same tissue type and $A_{\{tissue,NB\}}$ is the area segmented by the combination of Bevacizumab and Nivolumab.

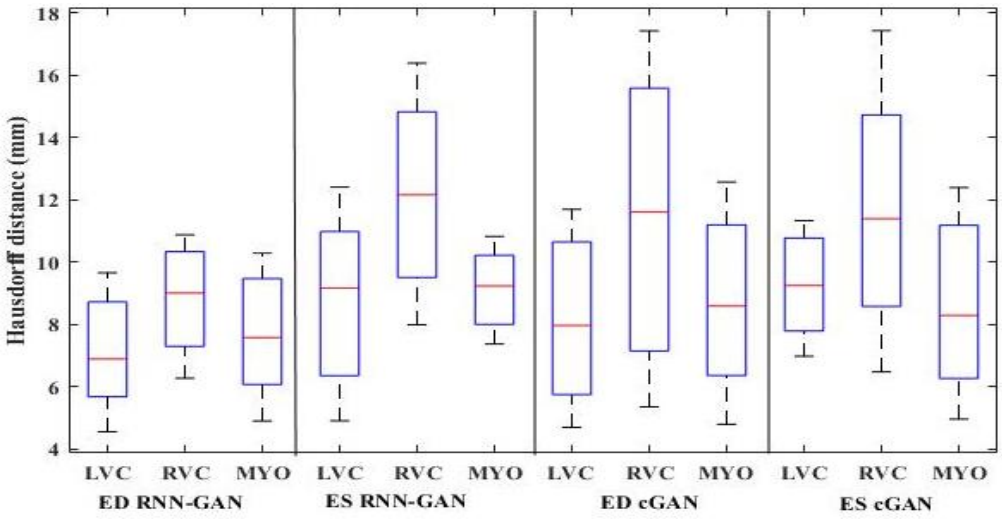

Figure 8: Hausdorff Distance of the Proposed Work

JOURNAL OF ALGEBRAIC STATISTICS
Volume 13, No. 3, 2022, p. 3894 - 3915
https://publishoa.com
ISSN: 1309-3452

Figure 8 depicted the Hausdorff distance of the proposed model. In order to govern the distance between segmentation boundaries, the Hausdorff distance was also calculated. The Hausdorff distance for ED RNN-GAN, ES RNN-GAN, ED cGAN, and ES cGAN. In one segmentation mask, the Hausdorff distance is the total distance between all points and the nearest point in the other segmentation mask.

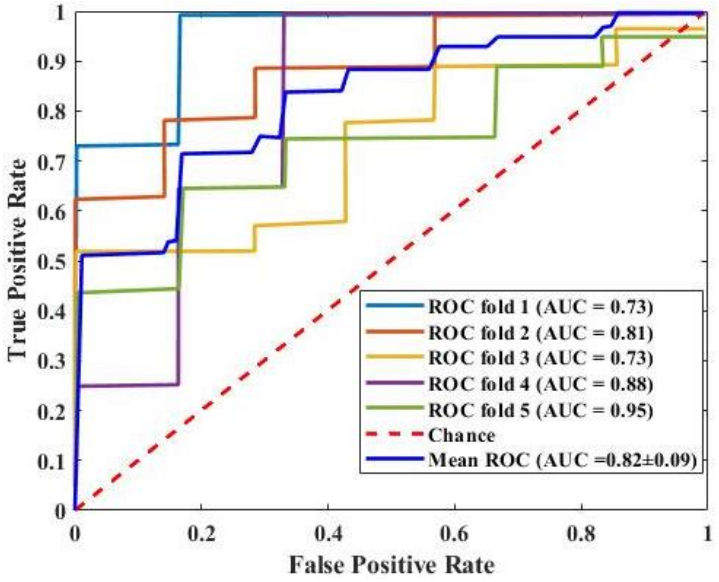

Figure 9: Local Recurrence Graph of Proposed Work

The local recurrence graph of the proposed method is depicted in figure 9. In this, the true positive rate (TPR) and the false positive rate (FPR) are calculated based on the ROC and AUC. Additionally, it depicted the ROC fold number as 1 to 5 and the AUC as 0.73, 0.81, 0.73, 0.88, and 0.95. Subsequently, the mean AUC is 0.82, and the TPR is gradually increased with the increasing false positive rate.

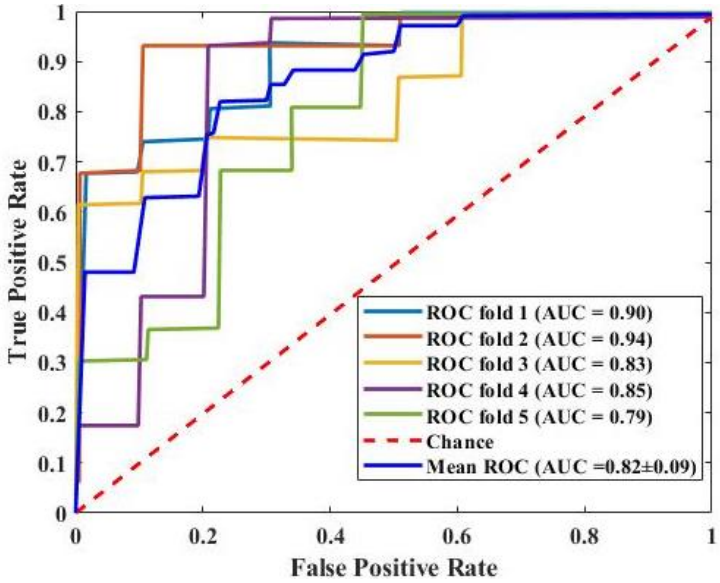

Figure 10: Distant Recurrence Graph of Proposed Work

Figure 10 represents the distant recurrence graph of the research work. Additionally, it consists of increasing the TPR by increasing the FPR. Besides the ROC curve, the corresponding AUC value for each method is also calculated and displayed. Subsequently, it portrays the AUC values as 0.90, 0.94, 0.83, 0.85, and 0.79 and the mean AUC value is 0.82, respectively.

JOURNAL OF ALGEBRAIC STATISTICS
Volume 13, No. 3, 2022, p. 3894 - 3915
https://publishoa.com
ISSN: 1309-3452

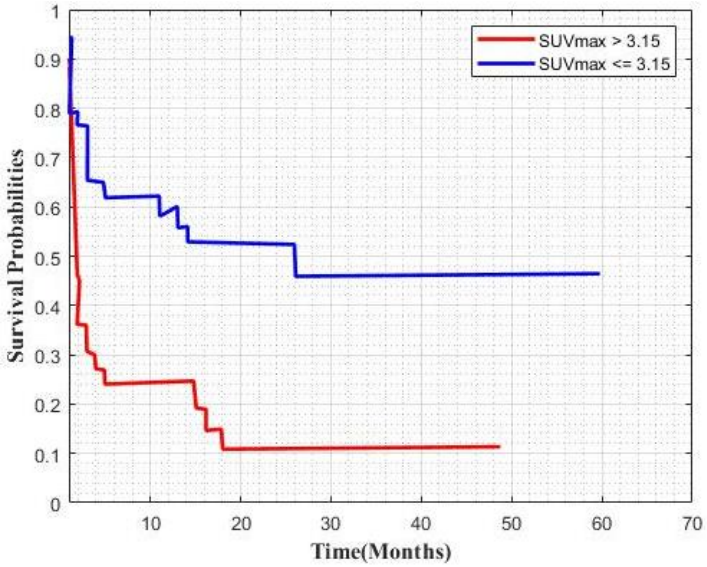

Figure 11: Survival Probability Graph 1

The Performance graph for survival probability is portrayed in figure 11. Additionally, it represents the standardised uptake value (SUV). The figure consists of two plots one is the maximum SUV of the figure is greater than 3.15 and the other is the maximum SUV is less than or equal to 3.15. Subsequently, it reveals that the maximum SUV is greater than 3.15 and produce a better survival probability than other.

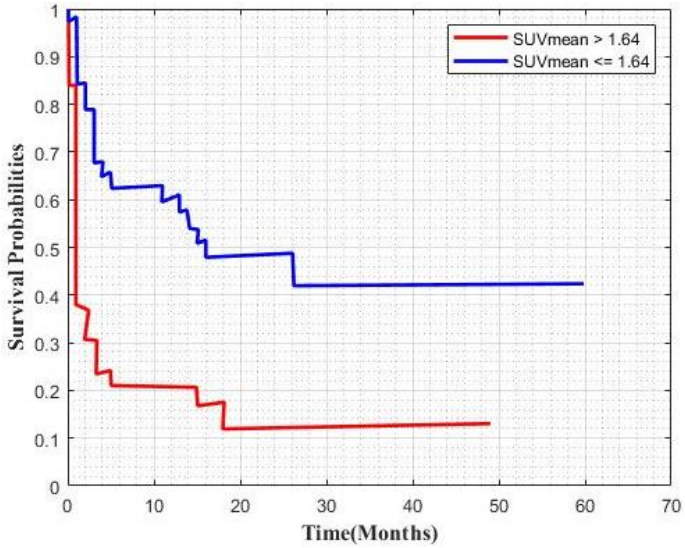

Figure 12: Survival Probability Graph 2

Figure 12 demonstrates the graph for mean survival probability. Subsequently, it consists of the mean SUV is greater than 1.64 and the mean SUV is less than or equal to 1.64. The mean probability value greater than 1.64 produce high probability than the other survival probability for different months, respectively.

JOURNAL OF ALGEBRAIC STATISTICS
Volume 13, No. 3, 2022, p. 3894 - 3915
https://publishoa.com
ISSN: 1309-3452

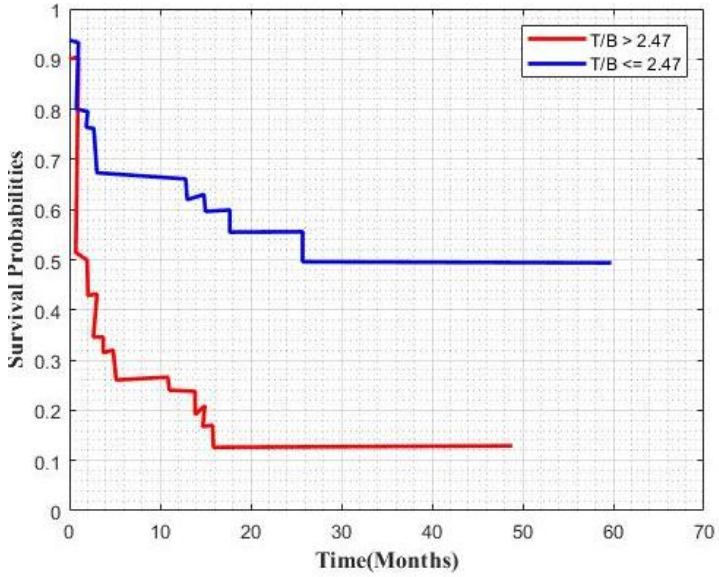

Figure 13: Survival Probability Graph 3

Figure 13 demonstrates the performance graph for survival probability for different months. Accordingly, it consists of two types; one is the SUV value is greater than 2.47 and the other one is less than or equal to 2.47. The survival probability of the work decreases with increasing months, subsequently, when the number of months increases, the survival probability decreases.

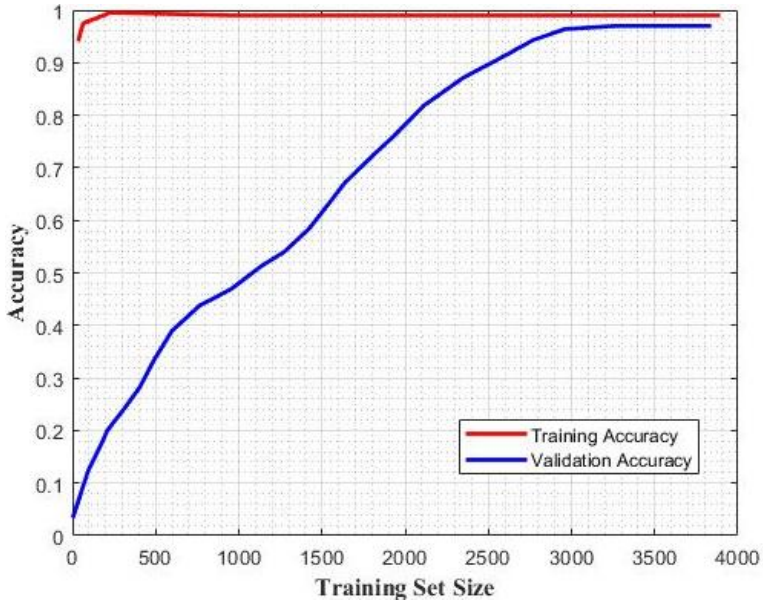

Figure 14: Performance Graph for Accuracy

The accuracy graph for the proposed work is illustrated in figure 14. The figure depicted the training and validation accuracy. Subsequently, it consists of training and testing accuracy. The training set size of the work is 0 to 4000. Consequently, it depicted that the training accuracy has a high accuracy value and the validation accuracy is gradually increased.

JOURNAL OF ALGEBRAIC STATISTICS
Volume 13, No. 3, 2022, p. 3894 - 3915
https://publishoa.com
ISSN: 1309-3452

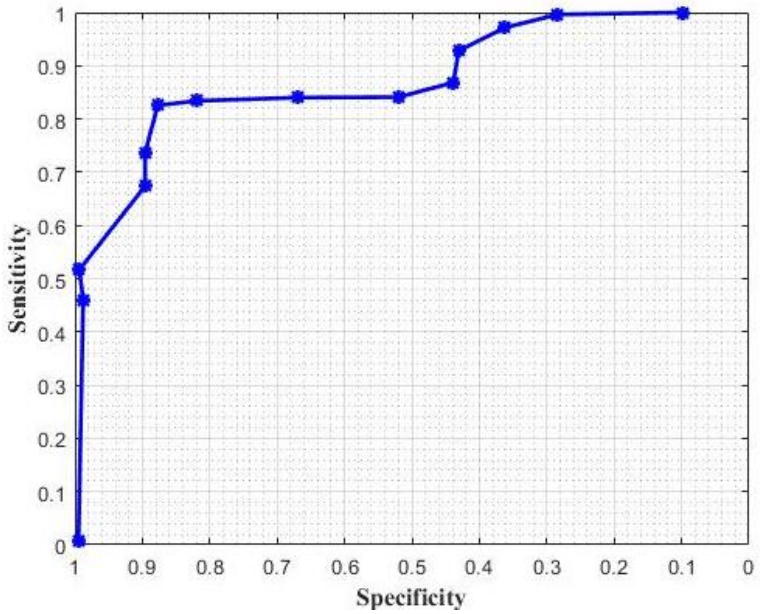

Figure 15: Sensitivity Vs Specificity Graph

Figure 15 portrays the specificity and sensitivity graph of the proposed method. Importantly, the sensitivity, and specificity of employing composite MAqCI scores to correctly identify short- and long-term survival patients markedly improved to ~98%. Subsequently, the sensitivity of the proposed work is increasing and the specificity of the research is also increased.

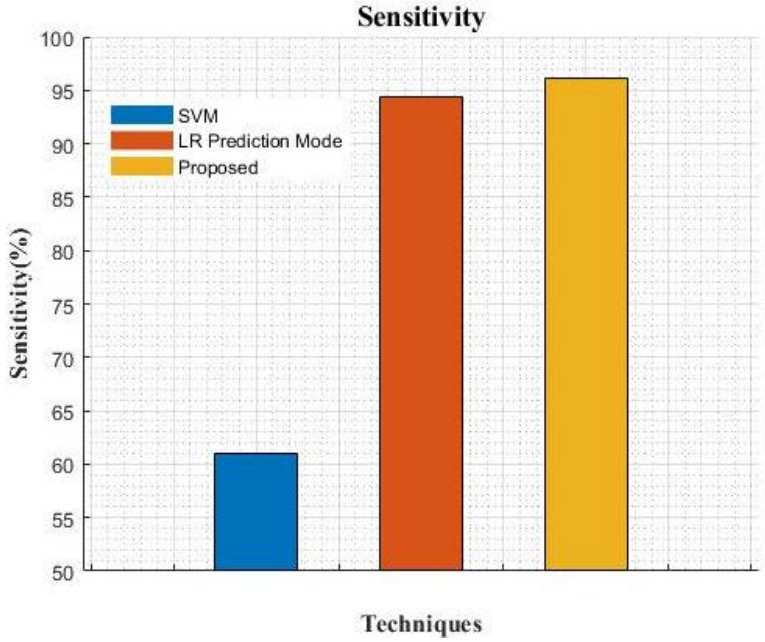

Figure 16: Comparison Graph for Sensitivity

The comparison graph for sensitivity is depicted in figure 16. Subsequently, the proposed model is compared with existing SVM [26], and local recurrence (LR) prediction mode [15] methods. The proposed technique yields higher performance than the other two existing methods, like 10% higher than the existing SVM method and 2% higher than the existing LR methods.

JOURNAL OF ALGEBRAIC STATISTICS
Volume 13, No. 3, 2022, p. 3894 - 3915
https://publishoa.com
ISSN: 1309-3452

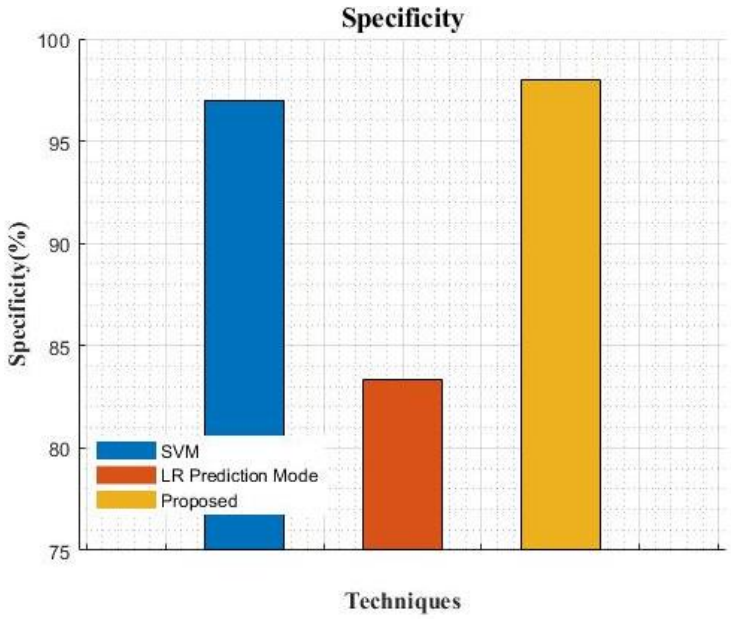

Figure 17: Comparison Graph for Specificity

The comparison graph for specificity is demonstrated in figure 17. Additionally, it depicts that the presented model is compared with the SVM and LR prediction models. The proposed method performs nearly 1% higher than the existing SVM methods and nearly 6% high than the existing LR prediction model.

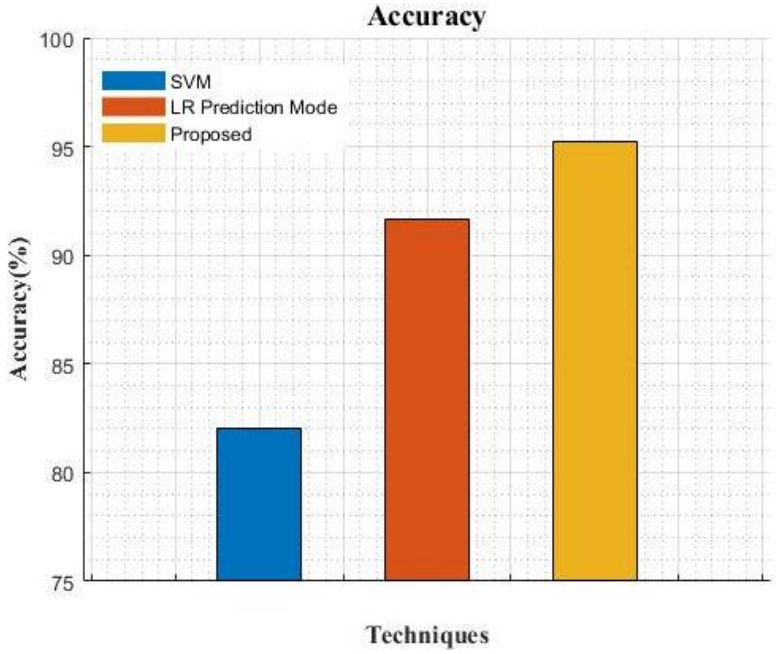

Figure 18: Comparison Graph for Accuracy

Figure 18 portrays the comparison graph for accuracy. The proposed method's accuracy is compared with SVM and LR methods. Subsequently, the proposed technique is 4% greater than the existing SVM method and 2% higher than the LR prediction models. Consequently, the proposed method has the best performance of the other methods.

6. CONCLUSION

Glioblastoma remains the most lethal brain tumour despite effective treatment, because of the high risk of recurrence. Clinical trials and treatment plans for distant recurrences differ from those for local recurrences because of

the significant genomic changes associated with distant recurrences. Tumour perfusional features are linked to prognosis, which is demonstrated by perfusion-weighted MRI. Subsequently, in glioblastoma recurrence risk prediction, very few research has been conducted, however, the glioblastoma recurrence patterns like local and distant recurrence. In this research, the machine learning technique of the Random Forest model and Deep Neural Network method is proposed to predict the glioblastoma recurrence risk. Initially, Resampling and Z-Score Normalisation are the images pre-processing that are used to remove bias and artefacts in neuroimaging data. The pre-processed image is then segmented using the Recurrent Neural Network-Generative Adversarial Network (RNN-GAN), which mitigates the impact of imbalanced pixel labels. Subsequently, the Wavelet Band-Pass Filtering technique is presented to extract the texture features and the CE-T1WI model predicts PFS and ORR in recurrent GBM patients treated with the combination of Nivolumab and Bevacizumab. Accordingly, Random Forest and DNN techniques are proposed for patients' recurrence risk. Additionally, a feature optimization algorithm like IBCGA has been introduced for patients' survival time prediction. The proposed techniques are evaluated using Python.

- The performance of the proposed work is recurrence prediction, survival probability, PFS, ORR, accuracy, specificity, and sensitivity. The proposed method is compared with existing SVM and LR prediction methods.
- The accuracy of the proposed method is 3% higher than the existing methods, the specificity of the work is approximately 4% higher than the existing methods, and the sensitivity of the proposed method is nearly 5% higher.

Subsequently, utilizing this proposed method, accurately predicts the glioblastoma recurrence risk and future research is needed to identify the unique immune microenvironment of the brain under tumour conditions respectively.

CONFLICT OF INTEREST: The authors do not have any Conflict of Interest.

ETHICAL APPROVAL: This article does not contain any studies with human participants or animals performed by any of the authors.

REFERENCES

[1] Wu, W., Klockow, J.L., Zhang, M., Lafortune, F., Chang, E., Jin, L., Wu, Y. and Daldrup-Link, H.E., 2021. Glioblastoma multiforme (GBM): An overview of current therapies and mechanisms of resistance. Pharmacological Research, 171, p.105780.

[2] Li, H., He, Y., Huang, L., Luo, H. and Zhu, X., 2020. The nomogram model predicting overall survival and guiding clinical decision in patients with glioblastoma based on the SEER database. Frontiers in Oncology, 10, p.1051.

[3] Chato, L. and Latifi, S., 2021. Machine Learning and Radiomic Features to Predict Overall Survival Time for Glioblastoma Patients. Journal of Personalized Medicine, 11(12), p.1336.

[4] Shim, K.Y., Chung, S.W., Jeong, J.H., Hwang, I., Park, C.K., Kim, T.M., Park, S.H., Won, J.K., Lee, J.H., Lee, S.T. and Yoo, R.E., 2021. Radiomics-based neural network predicts recurrence patterns in glioblastoma using dynamic susceptibility contrast-enhanced MRI. Scientific reports, 11(1), pp.1-14.

[5] Priya, S., Agarwal, A., Ward, C., Locke, T., Monga, V. and Bathla, G., 2021. Survival prediction in glioblastoma on post-contrast magnetic resonance imaging using filtration based first-order texture analysis: Comparison of multiple machine learning models. The neuroradiology journal, 34(4), pp.355-362.

[6] Ye, J., Huang, H., Jiang, W., Xu, X., Xie, C., Lu, B., Wang, X. and Lai, X., 2021. Tumor Grade and Overall Survival Prediction of Gliomas Using Radiomics. Scientific Programming, 2021.

[7] Zuo, S., Zhang, X. and Wang, L., 2019. A RNA sequencing-based six-gene signature for survival prediction in patients with glioblastoma. Scientific reports, 9(1), pp.1-10.

[8] Carvalho, B., Lopes, R.G., Linhares, P., Costa, A., Caeiro, C., Fernandes, A.C., Tavares, N., Osório, L. and Vaz, R., 2020. Hypertension and proteinuria as clinical biomarkers of response to bevacizumab in glioblastoma patients. Journal of Neuro-Oncology, 147(1), pp.109-116.

[9] Rathore, S., Akbari, H., Doshi, J., Shukla, G., Rozycki, M., Bilello, M., Lustig, R.A. and Davatzikos, C.A., 2018. Radiomic signature of infiltration in peritumoral edema predicts subsequent recurrence in glioblastoma: implications for personalized radiotherapy planning. Journal of Medical Imaging, 5(2), p.021219.

[10] Lee, M.H., Kim, J., Kim, S.T., Shin, H.M., You, H.J., Choi, J.W., Seol, H.J., Nam, D.H., Lee, J.I. and Kong, D.S., 2019. Prediction of IDH1 mutation status in glioblastoma using machine learning technique based on quantitative radiomic data. World neurosurgery, 125, pp. e688-e696.

[11] Kim, E.L., Sorokin, M., Kantelhardt, S.R., Kalasauskas, D., Sprang, B., Fauss, J., Ringel, F., Garazha, A., Albert, E., Gaifullin, N. and Hartmann, C., 2020. Intratumoral heterogeneity and longitudinal changes in gene expression predict differential drug sensitivity in newly diagnosed and recurrent glioblastoma. Cancers, 12(2), p.520.

[12] Hsieh, H.P., Wu, D.Y., Hung, K.C., Lim, S.W., Chen, T.Y., Fan-Chiang, Y. and Ko, C.C., 2022. Machine Learning for Prediction of Recurrence in Parasagittal and Parafalcine Meningiomas: Combined Clinical and MRI Texture Features. Journal of Personalized Medicine, 12(4), p.522.

[13] Lundemann, M., Munck af Rosenschöld, P., Muhic, A., Larsen, V.A., Poulsen, H.S., Engelholm, S.A., Andersen, F.L., Kjær, A., Larsson, H.B., Law, I. and Hansen, A.E., 2019. Feasibility of multi-parametric PET and MRI for prediction of tumour recurrence in patients with glioblastoma. European Journal of Nuclear Medicine and Molecular Imaging, 46(3), pp.603-613.

[14] Lukas, R.V., Rodon, J., Becker, K., Wong, E.T., Shih, K., Touat, M., Fassò, M., Osborne, S., Molinero, L., O'Hear, C. and Grossman, W., 2018. Clinical activity and safety of atezolizumab in patients with recurrent glioblastoma. Journal of neuro-oncology, 140(2), pp.317-328.

[15] Shim, K.Y., Chung, S.W., Jeong, J.H., Hwang, I., Park, C.K., Kim, T.M., Park, S.H., Won, J.K., Lee, J.H., Lee, S.T. and Yoo, R.E., 2020. Prediction of Recurrence Patterns in Glioblastoma Using DSC-MRI Radiomics-Based Deep Learning.

[16] Acquitter, C., Piram, L., Sabatini, U., Gilhodes, J., Moyal Cohen-Jonathan, E., Ken, S. and Lemasson, B., 2022. Radiomics-Based Detection of Radionecrosis Using Harmonized Multiparametric MRI. Cancers, 14(2), p.286.

[17] Mulford, K., McMahon, M., Gardeck, A.M., Hunt, M.A., Chen, C.C., Odde, D.J. and Wilke, C., 2022. Predicting Glioblastoma Cellular Motility from In Vivo MRI with a Radiomics Based Regression Model. Cancers, 14(3), p.578.

[18] Eisenhut, F., Engelhorn, T., Arinrad, S., Brandner, S., Coras, R., Putz, F., Fietkau, R., Doerfler, A. and Schmidt, M.A., 2021. A Comparison of Single-and Multiparametric MRI Models for Differentiation of Recurrent Glioblastoma from Treatment-Related Change. Diagnostics, 11(12), p.2281.

[19] Park, Y.W., Choi, D., Park, J.E., Ahn, S.S., Kim, H., Chang, J.H., Kim, S.H., Kim, H.S. and Lee, S.K., 2021. Differentiation of recurrent glioblastoma from radiation necrosis using diffusion radiomics with machine learning model development and external validation. Scientific reports, 11(1), pp.1-9.

[20] Ammari, S., Sallé de Chou, R., Assi, T., Touat, M., Chouzenoux, E., Quillent, A., Limkin, E., Dercle, L., Hadchiti, J., Elhaik, M. and Moalla, S., 2021. Machine-Learning-Based Radiomics MRI Model for Survival Prediction of Recurrent Glioblastomas Treated with Bevacizumab. Diagnostics, 11(7), p.1263.

[21] Wong, B.S., Shah, S.R., Yankaskas, C.L., Bajpai, V.K., Wu, P.H., Chin, D., Ifemembi, B., ReFaey, K., Schiapparelli, P., Zheng, X. and Martin, S.S., 2021. A microfluidic cell-migration assay for the prediction of progression-free survival and recurrence time of patients with glioblastoma. Nature biomedical engineering, 5(1), pp.26-40.

[22] Lee, S., Choi, S.H., Cho, H.R., Koh, J., Park, C.K. and Ichikawa, T., 2021. Multiparametric magnetic resonance imaging features of a canine glioblastoma model. Plos one, 16(7), p.e0254448.

[23] Shim, K.Y., Chung, S.W., Jeong, J.H., Hwang, I., Park, C.K., Kim, T.M., Park, S.H., Won, J.K., Lee, J.H., Lee, S.T. and Yoo, R.E., 2021. Radiomics-based neural network predicts recurrence patterns in glioblastoma using dynamic susceptibility contrast- enhanced MRI. Scientific reports, 11(1), pp.1-14.

[24] Lao, Y., Ruan, D., Vassantachart, A., Fan, Z., Jason, C.Y., Chang, E.L., Chin, R., Kaprealian, T., Zada, G., Shiroishi, M.S. and Sheng, K., 2021. Voxel-wise prediction of recurrent high grade glioma via proximity estimation coupled multi-dimensional SVM. International Journal of Radiation Oncology* Biology* Physics.

[25] Detti, B., Scoccianti, S., Teriaca, M.A., Maragna, V., Lorenzetti, V., Lucidi, S., Bellini, C., Greto, D., Desideri, I. and Livi, L., 2021. Bevacizumab in recurrent high-grade glioma: a single institution retrospective analysis on 92 patients. La radiologia medica, 126(9), pp.1249-1254.

[26] Petrova, L., Korfiatis, P., Petr, O., LaChance, D.H., Parney, I., Buckner, J.C. and Erickson, B.J., 2019. Cerebral blood volume and apparent diffusion coefficient–Valuable predictors of non-response to bevacizumab treatment in patients with recurrent glioblastoma. Journal of the neurological sciences, 405, p.116433.

[27] Disha Wankhede, Dr Selvarani Rangasamy," Review on Deep learning approach for brain tumor glioma analysis" International Conference on Convergence of Smart Technologies IC2ST-2021, https://doi.org/10.17762/itii.v9i1.144

[28] Trupti Vasantrao Bhandare, & Selvarani Rangasamy. (2021). Review on Heart Disease Diagnosis Using Deep Learning Methods. International Journal of Next-Generation Computing, 12(2), 91–102. https://doi.org/10.47164/ijngc.v12i2.206

[29] Vasantrao, BhandareTrupti & Rangasamy, Selvarani. (2021). Weighted Clustering for Deep Learning Approach in Heart Disease Diagnosis. International Journal of Advanced Computer Science and Applications. 12. 10.14569/IJACSA.2021.0120944.

[30] Disha Wankhede and Dr. Selvarani Rangasamy, "Dynamic Architecture Based Deep Learning Approach for Glioblastoma Brain Tumor Survival Prediction," Neurosci. Informatics, vol. 2, no. 4, p. 100062, 2022, doi: 10.1016/j.neuri.2022.100062.